# Collective resonant dynamics of the chiral spin soliton lattice in a monoaxial chiral magnetic crystal

F. J. T. Goncalves,[1,2,3,4,*] T. Sogo,[1] Y. Shimamoto,[1] Y. Kousaka,[2,3,5] J. Akimitsu,[2,3,5] S. Nishihara,[2,3] K. Inoue,[2,3,6] D. Yoshizawa,[3,7] M. Hagiwara,[3,7] M. Mito,[8] R. L. Stamps,[4] I. G. Bostrem,[9] Vl. E. Sinitsyn,[9] A. S. Ovchinnikov,[9,10] J. Kishine,[3,11] and Y. Togawa[1,3,4,12]

[1]*Department of Physics and Electronics, Osaka Prefecture University, 1-2 Gakuencho, Sakai, Osaka 599-8570, Japan*
[2]*Graduate School of Science, Hiroshima University, Higashi-Hiroshima, Hiroshima 739-8526, Japan*
[3]*Center for Chiral Science, Hiroshima University, Higashi-Hiroshima, Hiroshima 739-8526, Japan*
[4]*School of Physics and Astronomy, University of Glasgow, Glasgow G12 8QQ, United Kingdom*
[5]*Department of Physics and Mathematics, Aoyama Gakuin University, Sagamihara, Kanagawa 252-5258, Japan*
[6]*IAMR, Facility of Science, Hiroshima University, Higashi-Hiroshima, Hiroshima 739-8530, Japan*
[7]*Center for Advanced High Magnetic Field Science, Graduate School of Science, Osaka University, Toyonaka, Osaka 560-0043, Japan*
[8]*Graduate School of Engineering, Kyushu Institute of Technology, Kitakyushu 804-8550, Japan*
[9]*Institute of Natural Sciences, Ural Federal University, Ekaterinburg 620083, Russia*
[10]*Institute for Metal Physics, Ural Division of RAS, Ekaterinburg 620137, Russia*
[11]*Division of Natural and Environmental Sciences, The Open University of Japan, Chiba 261-8586, Japan*
[12]*JST, PRESTO, 4-1-8 Honcho Kawaguchi, Saitama 333-0012, Japan*

(Received 14 November 2016; revised manuscript received 13 January 2017; published 14 March 2017)

The magnetic resonance properties of microsized monoaxial chiral crystals of $CrNb_3S_6$ are investigated. We observed that the resonance of the chiral soliton lattice is sensitive to the polarization of the driving microwave field. When the microwave field is parallel to the helical axis, the resonance is symmetric with regards to the magnetic field direction. In contrast, asymmetric field dependence emerges when the microwave field is perpendicular to the helical axis. The robustness of the chiral magnetic order, due to topological protection, allows tuning the resonance frequency in ways hardly accessible using nanopatterned films.

DOI: 10.1103/PhysRevB.95.104415

The chiral nature of matter has attracted immense attention recently as it can provide novel ways of manipulating the propagation of electromagnetic waves whose frequency spans from the megahertz to the terahertz regime [1–3]. In particular, chiral helimagnets can be seen as naturally occurring nanostructured materials whose physical properties are quantized and topologically protected via the formation of a chiral spin soliton lattice (CSL), which can be highly reconfigurable in the presence of an external magnetic field. Such characteristics emerge due to a strong link between the crystalline structure and the magnetic texture. Advances in this field are motivated by exploring novel concepts for spin electronics using chiral helimagnets as spin-wave media for applications in information storage, processing, and filtering [4–9]. In addition, the discreteness found in the magnetization and magnetoresistance (MR) can be seen as multistate memory cells [10–13], and the spin-wave properties are expected to allow nonreciprocal effects with which one can control spin-wave propagation [14,15] and interference [16]. Moreover, theoretical results suggest that the CSL in motion can generate a voltage signal [17,18], which can be amplified as a result of the collective resonance in a confined geometry [19]. This effect is referred to as spin motive force.

The first direct experimental evidence for the formation of the CSL was presented in Ref. [20], where Lorentz microscopy was employed to image the soliton lattice in a monoaxial chiral helimagnet, $CrNb_3S_6$. It was found that the soliton density acts as an order parameter of the CSL formation as a function of the applied magnetic field. This result was followed by a sequence of studies devoted to the nontrivial response of the system [12,13,21–23]. In particular, the MR data correlated well with the quantized nature of the CSL density in the confinement of a micrometer-sized crystal [12]. These developments suggest that the robustness and phase coherence of the CSL, unique to the monoaxial chiral crystal, play an important role in defining the resonance properties [19,24] we propose to investigate.

In this paper we present the fundamental resonance properties of $CrNb_3S_6$ microsized lamellae, investigated experimentally as a function of a magnetic field applied perpendicular to the helical axis ($c$ axis). This field configuration allows tuning of the resonance frequency of the CSL while maintaining its phase coherence. We found a clear difference between the forced ferromagnetic (F-FM) and the CSL phase: While the resonance of the F-FM phase was independent of the field sweep direction, the CSL phase exhibited a hysteresis effect, followed by a highly nonlinear resonance behavior in the vicinity of the critical field. Importantly, it was found that in the CSL phase, the resonance is largely affected by the orientation of the driving microwave field with respect to the helical axis of the crystal. We note that the available theory of spin resonance in bulk monoaxial chiral helimagnets also predicts different forms of resonance signals depending on the orientation of the microwave and the steady magnetic fields [24]. However, this is related to the differences between the spin-wave spectra in the conical and soliton lattice phases which appear under an external magnetic field applied parallel and perpendicular to the $c$ axis, respectively. More recent work, devoted to the study of the magnetic order and MR in micrometer-sized crystals, has revealed that the confinement effects emerge due to the macroscopic coherence of the CSL

*f-goncalves@pe.osakafu-u.ac.jp

 

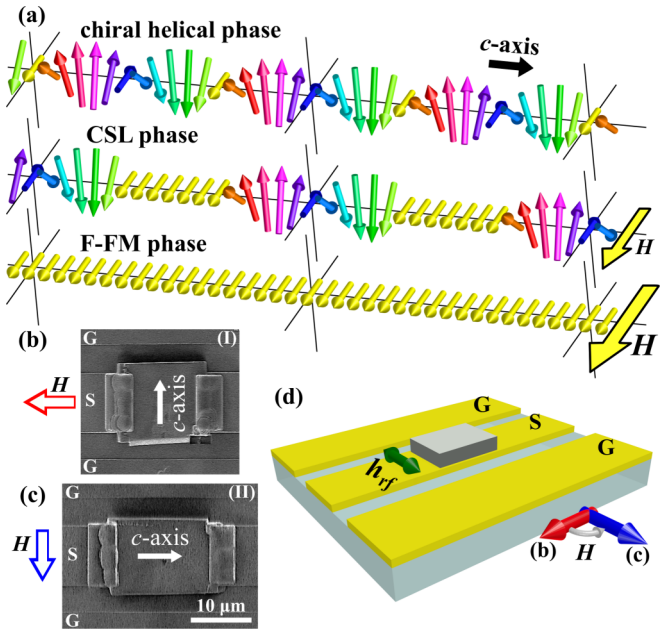


FIG. 1. (a) Illustration of the spin textures associated with the chiral helical, CSL, and F-FM phases. Scanning ion microscopy images show the direction of the $c$ axis with regards to the signal line of the CPW for (b) (I) and (c) (II). Dimensions of the lamella used in (I) and (II) are 13.9 and 13.0 $\mu$m for the direction parallel to the $c$ axis and 15.2 and 20.0 $\mu$m direction perpendicular to the $c$ axis, respectively. The thickness of the lamellae used in (I) and (II) is 500 nm. (d) Schematic illustration of the lamella, $H$, and $h_{\mathrm{rf}}$ with regards to the ground (G) and signal (S) of the CPW.

and the pinning effect at the boundaries of either the crystalline domains with different chirality or specimen edges [12]. The effect of pinning fields on the collective resonance dynamics is not yet well understood from a theoretical standpoint [19]. In our study we demonstrate the emergence of different resonance properties due to confinement as these have not been observed in bulk crystals. We believe that these experimental findings may shed light on the nontrivial aspects of the collective resonant dynamics of nonlinear, tunable, and phase-coherent CSL.

Of interest to our work is the monoaxial chiral crystal $CrNb_3S_6$, whose structure consists of hexagonal planes of $Nb_3S_6$ stacked along the $c$ axis and intercalated with Cr atoms. $CrNb_3S_6$ bulk crystals are grown using a chemical vapor transport method [25,26]. Below a critical temperature $T_c = 127$ K, and for an external field $H = 0$, a chiral helical phase appears with a period of 48 nm as a result of the competing Heisenberg exchange and antisymmetric Dzyaloshinskii-Moriya interactions along the $c$ axis [27], while below a critical field $H_c$, the chiral helical phase transforms to a chiral helicoidal phase consisting of a periodic spin arrangement of $2\pi$ twists partitioned by F-FM regions [28,29]. Due to its robustness the helicoidal phase is frequently referred to as a CSL phase. At $H_c$ the incommensurate CSL phase evolves to a commensurate F-FM phase [27]. These three magnetic phases are schematically illustrated in Fig. 1(a). When $H$ is applied perpendicular to the $c$ axis, $H_c$ may range from 0.1 to 0.3 T, depending on the crystal quality and alignment between $H$ and the magnetization plane [12]. When $H$ is applied parallel to the $c$ axis, the conical phase transforms into the F-FM phase at an $H_c$ of 2 T. Such a difference in $H_c$ arises from a strong anisotropy with its origin in the interlayer and intralayer exchange coupling terms [27]. As a result, the magnetic moment is confined to a magnetization plane, $ab$ plane, and a quasi-one-dimensional model is sufficient to describe the physical properties of the system [30].

Figures 1(b)–1(d) illustrate the two experimental configurations (I) and (II), with the key difference being the angle between the $c$ axis of the crystal and the polarization of the microwave field $h_{\mathrm{rf}}$ generated in the coplanar waveguide (CPW). In (I) the $c$ axis is parallel to $h_{\mathrm{rf}}$ while in (II) the $c$ axis is perpendicular to $h_{\mathrm{rf}}$. We assume that the magnetization precession is driven by the component of the $h_{\mathrm{rf}}$ perpendicular to the axis of the signal line, in the plane of the substrate. The CPWs were fabricated on a large $Al_2O_3$ substrate using electron beam lithography and evaporation of Au (200 nm thickness). Each lamella was cut from the bulk crystal using a focused ion beam and attached to the signal line of a CPW using tungsten deposition.

Broadband frequency magnetic resonance experiments were carried out using a vector network analyzer (VNA) connected to the ports of a cryogenic microwave probe station. Inside the cryogenic chamber a pair of microwave probes made contact with the CPW containing each of the specimens. The resonance line shape was obtained by measuring the forward transmission parameter $S_{21}$ as a function of frequency (0.1–40 GHz) in the VNA for different values of $H$. Two sets of Helmholtz coils generate the in-plane vector $H$ with a maximum magnitude of 0.2 T.

Figure 2 presents several examples of the experimental data corresponding to (I) and (II), obtained at 50 K. The spectra were acquired while $H$ was swept from 200 to $-200$ mT. The solid symbols in (I) and (II) highlight the resonance peaks varying as a function of $H$. At a postmeasurement stage, the spectrum obtained at 78 mT was used for subtraction of the nonmagnetic background, $S_{21}(H) - S_{21}(78\ \mathrm{mT})$, therefore its position (black arrows) is fixed on all data shown.

The resonance frequency in the F-FM phase, at 200 mT, is found to be the same for (I) and (II). However, in the CSL phase both configurations exhibit distinct behavior in terms of resonance position and the number of peaks. For instance, at 0 mT, the resonance frequency in (I) is 19.63 GHz while in (II) two modes are observed at 17.25 and 19.93 GHz. Interestingly, at $-120$ mT, two modes appear on both configurations but at different frequencies. As for the resonance intensity, in (I) the amplitude is larger in the F-FM than in the CSL phase, while the opposite is found in (II). For example, at 200 mT the amplitude of the resonance peak in (I) is larger by a factor of 2 when compared to the resonance peak in (II).

Figure 3(a) shows the field dependence of the resonance frequencies in (I). The data set designated by a negative field sweep was obtained while varying $H$ from 200 to $-200$ mT and the data set designated by a positive field sweep was obtained while sweeping $H$ from $-200$ to 200 mT.

As exemplified by the negative field sweep, the square-root dependence of the resonance frequency found at large $H$, where the F-FM phase is formed, is qualitatively consistent with the behavior observed in the F-FM phase of $CrNb_3S_6$

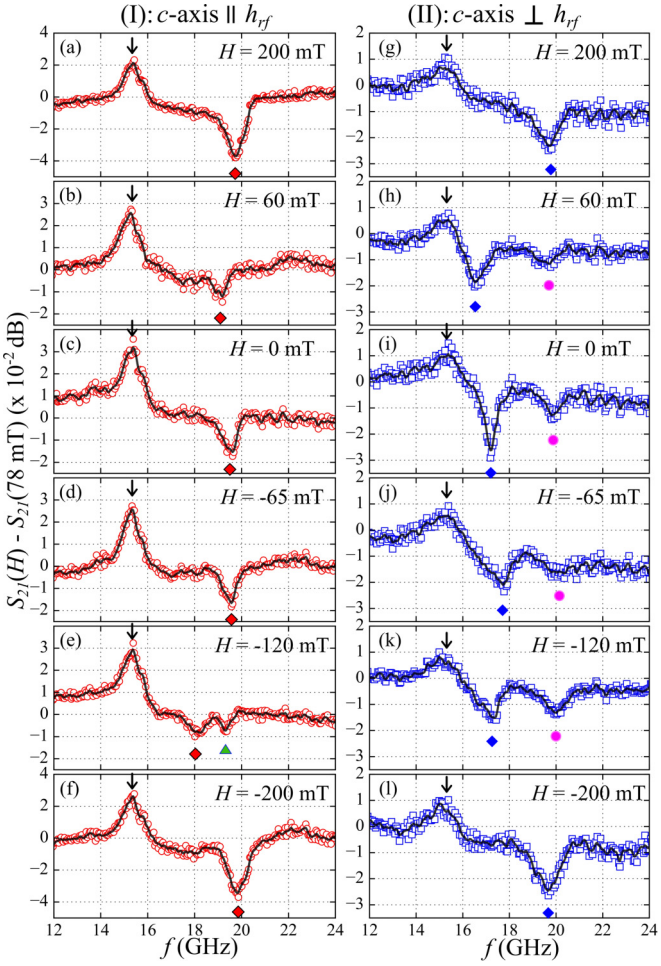


FIG. 2. Corrected $S_{21}$ parameter as a function of frequency in (I) and (II) at different $H$. The open symbols and the continuous lines represent the raw and smoothed experimental data, respectively. The solid symbols indicate the position of the resonance peaks. The black arrows indicate the resonance of the reference spectra.

in the bulk crystal with $H$ parallel to the $c$ axis [31]. In general, the dependence in the F-FM phase can be seen as the response of a saturated state in a FM material with a saturation magnetization of 0.2 T [21,26,32] and an effective anisotropy which stems from the easy-plane anisotropy of the crystal and demagnetization fields due to the shape of the crystal.

While decreasing $H$ towards the CSL phase, an abrupt frequency jump of 3.9 GHz occurs at 76 mT, indicating the transition from the F-FM phase to the CSL phase. At small $H$ the resonance frequency becomes almost independent of the magnitude of $H$. When approaching $H_c = -134$ mT, when a change in soliton number or density of the CSL phase is expected, a pronounced decrease is found in the resonance frequency. The obtained value for $H_c$ is consistent with that reported in Ref. [32].

The positive field sweep exhibits a mirrored symmetry of the negative field sweep. For clarity, this characteristic is demonstrated in Fig. 3(a) by comparing the sweeps for $H > 0$ mT.

In the transition from F-FM to CSL, shown in Fig. 3(b), two resonance modes exist in the field range between 72 and 76 mT. At 76 mT the lowest resonance frequency, extrapolated from the F-FM phase, shows a 30% decrease of the intensity with a simultaneous emergence of a different resonance at 19 GHz, which connects smoothly with the mode found in the CSL phase. The intensity ratio between these two modes is maintained until $H$ is decreased to 72 mT, at which point the resonance mode at lower frequency vanishes completely while the resonance amplitude corresponding to the CSL phase increases up to the values observed at smaller fields. It is noted that the coexistence of the CSL and F-FM phases could not be observed in the MR data [12,21] which correlated to a well-defined soliton density, suggesting the emergence of fluctuations in the spin dynamics near the transition to the CSL phase.

Figure 3(c) focuses on the transition from CSL to F-FM, where two resonance modes are observed. On both sweep directions the field dependence is described by a gradual decrease in the frequency of the main resonance mode with a simultaneous emergence of a second mode at a higher frequency, at 110 mT. The resonance frequency of the main mode gradually decreases to 15.8 GHz until 134 mT, but with further increasing $H$ the resonance frequency exhibits a square-root dependence, indicating the emergence of the F-FM phase. This field dependence of the resonance frequency may be a manifestation of a magnetostatic mode in the thin plate [33]. In contrast, a pronounced linear stepwise increase in the resonance frequency is observed in the second mode until vanishing at 144 mT. Within the field range where two modes coexist a slight difference is observed in the resonance between the negative and positive field sweeps. Indeed, in the positive sweep the main mode evolves from the CSL to the F-FM phase at 132 mT, and the second mode occurs at a higher resonance frequency and vanishes at 140 mT. Different field sweeps showed marginal variations in the resonance frequency and $H$ of the second mode, suggesting a field history dependence possibly due to the vanishing of the solitons near the edges of the lamella.

In summary, the resonance behavior of the CSL in (I) is consistent with the corresponding ground-state configuration described using MR and Lorentz transmission electron microscopy (TEM) data [12,21]: The decreasing branch contained a sharp jump of the resonance frequency and MR data as a result of the abrupt transition from F-FM to CSL phase; in the increasing branch, the gradually decreasing resonance frequency of the main mode follows the same dependence of the MR data, which correlates well with the reduction of the soliton density in a confined specimen. The resonance mode emerging in the CSL phase does not follow the conventional Kittel approach and therefore requires a model considering the collective resonance excitation in a spatially confined system while including the role of the Dzyaloshinskii-Moriya interaction in setting the ground state [19,24]. In qualitative terms, the resonance frequency of the main mode, in the field region from 0 T until $H_c$, decreases rapidly when approaching $H_c$, following the reduction in the soliton density.

Figure 4 shows the field dependence of the resonance modes obtained in (II). In the F-FM phase, the square-root decrease in the resonance frequency with decreasing $H$ is quantitatively the same as in (I). Moreover, the field range over which the CSL phase exists is 225 mT in (I) while it is 205 mT in

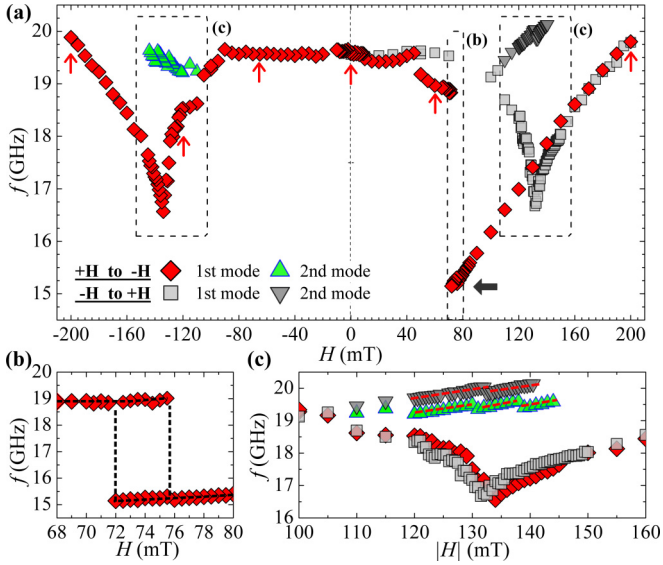


FIG. 3. (a) Resonance frequency as a function of $H$ in (I). Diamond and triangle-up markers correspond to the negative field sweep. The square and triangle-down markers correspond to the positive field sweep. Vertical solid arrows indicate the resonance position corresponding to the data of Figs. 2(a)–2(f). The horizontal arrow represents the position of the reference spectrum. The transitions from F-FM to CSL and CSL to F-FM are shown in (b) and (c), respectively. The dashed lines illustrate the stepped dependence of the resonance frequency. The average fitting error in measuring the resonance peaks is 100 MHz in the F-FM and CSL phases, while near $H_c$ the error is 200 MHz. Data acquired with a field step of 5 mT, except in the vicinity of 78 mT in (b) and −130 mT in (c) where the field step was 1 or 0.5 mT.

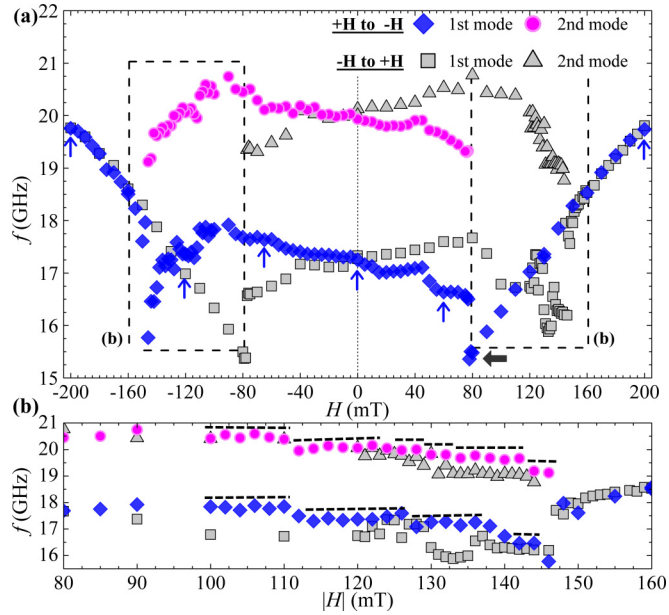


FIG. 4. (a) Resonance frequency as a function of $H$ in (II). The diamonds and circles correspond to the negative field sweep while the squares and triangles correspond to the positive field sweep. The vertical arrows indicate the resonance position corresponding to the data shown in Figs. 2(g)–2(l). The horizontal arrow indicates the position of the reference spectrum. (b) Details of the transition from CSL to F-FM. The dashed lines illustrate the stepwise behavior of the resonance frequency. The average fitting error in measuring the resonance peaks is 100 MHz in the F-FM and CSL, while near $H_c$ the error is 200 MHz.

(II). These findings suggest that the marginal difference in the shape of the microsized crystal has a negligible contribution to resonance properties.

However, the resonance behavior in the CSL phase of (II) is clearly different from that observed in (I). The first noticeable difference is the existence of two resonance modes across the entire CSL phase. For instance, in the negative field sweep, both modes emerge at 78 mT and vanish at −145 mT, with the main difference being that the second mode is shifted upwards in resonance frequency by 3 GHz. Below −145 mT, the monotonous increase of the resonance frequency indicates the transformation into the F-FM phase, as observed in (I).

Second, in the CSL phase the resonance frequency of both modes increases linearly with the field sweep and is thus pronouncedly asymmetric with regards to $H = 0$. For instance, in the negative field sweep, between 78 and −100 mT, the resonance frequency of both modes increases almost linearly by 1.8 GHz, resulting in an unusual hysteresis in the resonance with the field sweep direction. This sloped behavior is not observed in (I) and does not correlate directly with the variation in the soliton density.

Third, both resonance modes in the CSL phase exhibit a stepwise behavior with a typical frequency jump of 0.33 GHz between each of the plateaus. This behavior is more pronounced near $H_c$ of both negative and positive field sweeps, as shown in Fig. 4(b). An explanation of these properties is currently unavailable.

By comparing the results of the CSL phase in (I) and (II), it is clear that the collective resonance response is highly dependent on the direction of the excitation field with regards to the helical axis. When the microwave field is perpendicular to the $ab$ plane, the resonance is symmetric around $H = 0$. In contrast, when the microwave field is parallel to the $ab$ plane, the resonance modes become asymmetric with regards to $H$. We stress that in previous work, the MR data were found to strongly correlate with the ground-state configuration observed using Lorentz microscopy [12], matching the behavior of (I). However, in (II) the excitation field is driving the dynamics of the CSL in a way that does not evidently correlate to its ground state. Moreover, we note that the observation of a resonance in (II) contrasts with conventional ferromagnetic thin films, where the linear dynamic response along the magnetization is largely suppressed. Although the mechanism is not clear, it hints for the need of using a model considering the noncollinear spin arrangement upon excitation of microwave fields within the $ab$ plane.

We demonstrate that the robustness and coherence of the CSL extends also to the gigahertz regime in the form of collective resonance. With the choice of the polarization of the excitation field, one is able to tune the symmetry of the resonance response, making the CSL phase useful for polarization selective devices. The degree of reconfigurability achieved with the CSL may be functionalized towards controlling and manipulating spin-wave propagation, reflection, and interference.

We thank Y. Kato for fruitful discussions. This work was supported by JSPS Grant-in-Aid for Scientific Research (S) (No. 25220803), JSPS Core-to-Core Program "Advanced Research Networks", Act 211 Government of the Russian Federation No. 02.A03.21.0006, and by the Ministry of Education and Science of the Russian Federation, Grant No. MK-6230.2016.2 and Grant RFBR 17-52-50013.

[1] M. Menzel, Y. Mokrousov, R. Wieser, J. E. Bickel, E. Vedmedenko, S. Blügel, S. Heinze, K. von Bergmann, A. Kubetzka, and R. Wiesendanger, Phys. Rev. Lett. **108**, 197204 (2012).
[2] V. K. Valev, J. J. Baumberg, C. Sibilia, and T. Verbiest, Adv. Mater. **25**, 2517 (2013).
[3] T. Schwarze, J. Waizner, M. Garst, A. Bauer, I. Stasinopoulos, H. Berger, C. Pfleiderer, and D. Grundler, Nat. Mater. **14**, 478 (2015).
[4] R. Hertel, W. Wulfhekel, and J. Kirschner, Phys. Rev. Lett. **93**, 257202 (2004).
[5] G. Duerr, R. Huber, and D. Grundler, J. Phys.: Condens. Matter **24**, 024218 (2012).
[6] J. H. Lee, D. Petit, R. Lavrijsen, A. Fernández-Pacheco, R. Mansell, and R. P. Cowburn, Appl. Phys. Lett. **104**, 232404 (2014).
[7] M. Vogel, A. V. Chumak, E. H. Waller, T. Langner, V. I. Vasyuchka, B. Hillebrands, and G. von Freymann, Nat. Phys. **11**, 487 (2015).
[8] K. Wagner, A. Kákay, K. Schultheiss, A. Henschke, T. Sebastian, and H. Schultheiss, Nat. Nanotechnol. **11**, 432 (2016).
[9] X. Xing and Y. Zhou, NPG Asia Mater. **8**, e246 (2016).
[10] M. N. Wilson, E. A. Karhu, A. S. Quigley, U. K. Rößler, A. B. Butenko, A. N. Bogdanov, M. D. Robertson, and T. L. Monchesky, Phys. Rev. B **86**, 144420 (2012).
[11] J.-I. Kishine, I. G. Bostrem, A. S. Ovchinnikov, and V. E. Sinitsyn, Phys. Rev. B **89**, 014419 (2014).
[12] Y. Togawa, T. Koyama, Y. Nishimori, Y. Matsumoto, S. McVitie, D. McGrouther, R. L. Stamps, Y. Kousaka, J. Akimitsu, S. Nishihara, K. Inoue, I. G. Bostrem, V. E. Sinitsyn, A. S. Ovchinnikov, and J. Kishine, Phys. Rev. B **92**, 220412(R) (2015).
[13] K. Tsuruta, M. Mito, Y. Kousaka, J. Akimitsu, J.-i. Kishine, Y. Togawa, H. Ohsumi, and K. Inoue, J. Phys. Soc. Jpn. **85**, 013707 (2016).
[14] S. Seki, Y. Okamura, K. Kondou, K. Shibata, M. Kubota, R. Takagi, F. Kagawa, M. Kawasaki, G. Tatara, Y. Otani, and Y. Tokura, Phys. Rev. B **93**, 235131 (2016).
[15] Y. Iguchi, S. Uemura, K. Ueno, and Y. Onose, Phys. Rev. B **92**, 184419 (2015).
[16] C. Schütte and M. Garst, Phys. Rev. B **90**, 094423 (2014).
[17] J.-i. Kishine, I. G. Bostrem, A. S. Ovchinnikov, and V. E. Sinitsyn, Phys. Rev. B **86**, 214426 (2012).
[18] A. S. Ovchinnikov, V. E. Sinitsyn, I. G. Bostrem, and J. Kishine, J. Exp. Theor. Phys. **116**, 791 (2013).
[19] J.-i. Kishine, I. Proskurin, I. G. Bostrem, A. S. Ovchinnikov, and V. E. Sinitsyn, Phys. Rev. B **93**, 054403 (2016).
[20] Y. Togawa, T. Koyama, K. Takayanagi, S. Mori, Y. Kousaka, J. Akimitsu, S. Nishihara, K. Inoue, A. S. Ovchinnikov, and J. Kishine, Phys. Rev. Lett. **108**, 107202 (2012).
[21] Y. Togawa, Y. Kousaka, S. Nishihara, K. Inoue, J. Akimitsu, A. S. Ovchinnikov, and J. Kishine, Phys. Rev. Lett. **111**, 197204 (2013).
[22] K. Tsuruta, M. Mito, H. Deguchi, J. Kishine, Y. Kousaka, J. Akimitsu, and K. Inoue, Phys. Rev. B **93**, 104402 (2016).
[23] Y. Togawa, Y. Kousaka, K. Inoue, and J.-i. Kishine, J. Phys. Soc. Jpn. **85**, 112001 (2016).
[24] J.-i. Kishine and A. S. Ovchinnikov, Phys. Rev. B **79**, 220405 (2009).
[25] T. Moriya and T. Miyadai, Solid State Commun. **42**, 209 (1982).
[26] Y. Kousaka, Y. Nakao, J. Kishine, M. Akita, K. Inoue, and J. Akimitsu, Nucl. Instrum. Methods Phys. Res., Sect. A **600**, 250 (2009).
[27] J.-i. Kishine and A. Ovchinnikov, in *Solid State Physics*, 1st ed. (Elsevier, Amsterdam, 2015), pp. 1–130.
[28] I. E. Dzyaloshinskii, Sov. Phys. JETP **19**, 960 (1964).
[29] P. de Gennes, Solid State Commun. **88**, 1043 (1993).
[30] M. Shinozaki, S. Hoshino, Y. Masaki, J.-i. Kishine, and Y. Kato, J. Phys. Soc. Jpn. **85**, 074710 (2016).
[31] D. Yoshizawa, J.-i. Kishine, Y. Kousaka, Y. Togawa, M. Mito, J. Akimitsu, K. Inoue, and M. Hagiwara, Phys. Proc. **75**, 926 (2015).
[32] T. Miyadai, K. Kikuchi, H. Kondo, S. Sakka, M. Arai, and Y. Ishikawa, J. Phys. Soc. Jpn. **52**, 1394 (1983).
[33] A. I. Akhiezer, V. G. Bar'yakhtar, and S. V. Peletminskii, in *Spin Waves*, edited by S. Doniach (North-Holland Publishing Co., Amsterdam, 1968).